Interferometer density measurements of a high-velocity plasmoid

A. Case, S. Messer, R. Bomgardner, and F. D. Witherspoon
HyperV Technologies Corp., Chantilly, Virginia 20151, USA

(Received 8 December 2009; accepted 8 April 2010; published online 7 May 2010)

The plasmoid produced by a half-scale contoured gap coaxial plasma accelerator using ablative polyethylene capillary plasma injectors is measured using a quadrature heterodyne HeNe interferometer. The plasmoid is found to have a sharp rise in density at the leading edge, with a gradual falloff after the peak density. For this early test series, an average bulk density of 5×10^{14} cm^{-3} is observed, with densities up to 8×10^{14} cm^{-3} seen on some shots. Although plasmoid mass is only about 58 μg due to the low current and injected mass used in these tests, good shot-to-shot repeatability is attained making analysis relatively straightforward, thus providing a solid foundation for interpreting future experimental results. © *2010 American Institute of Physics*. [doi:10.1063/1.3420207]

I. INTRODUCTION

Coaxial plasma accelerators[1] are widely used to drive high velocity plasmoids.[2] A new approach to this technology is being experimentally developed[3] that utilizes contoured electrodes and careful control of plasma microphysics to increase both the mass and velocity of the plasmoids produced. Simulations have shown[3,4] that electrode shaping, coupled with injection of a preionized plasma armature (as opposed to the traditional technique of feeding the armature by snowplowing up a neutral gas prefill) will allow total masses of 200 μg to be accelerated to velocities of 200 km/s in a full-scale gun operating at ~1 MA.

HyperV Technologies Corp. is developing these contoured gap coaxial plasma accelerators as a driver for magnetoinertial fusion (MIF) as well as for potential applications in refueling,[5] disruption mitigation, spacecraft propulsion,[6–8] momentum injection,[9] and materials processing. The plasma gun used to produce the plasmoids discussed here is a one-half scale prototype of an accelerator ultimately designed as a driver for MIF experiments.

The accelerator consists of a ring of 32 ablative polyethylene capillaries which inject a preionized plasma armature into the breech of the coaxial section of the accelerator. In the coaxial section a radial current sheet drives the armature down the accelerator via magnetic pressure until it reaches the end of the inner electrode, where the attachment point of the current sheet moves to the tip of the inner electrode while the outer electrode attachment point continues down the accelerator, leading to a pinching of the plasma armature in a manner similar to a plasma focus. The final pinching of the plasma increases density and plasmoid velocity. The acceleration process therefore has three phases occurring in three sections of the accelerator: injection, coaxial acceleration, and pinching.

Details of the device are contained in Witherspoon *et al.*[3] 2009. In the following, we focus on the interferometer diagnostic for our plasma jet research, and present measurements and analysis of a particularly well characterized early test series produced by the half-scale gun in November 2007. Even though plasmoid mass in these tests is low, in fact only about 58 μg, the chosen test series shows good reproducibility and is readily analyzed, thus providing a solid foundation for interpreting future experimental results.

II. EXPERIMENTAL ARRANGEMENT

The system used here is a HeNe quadrature heterodyne interferometer broadly based on the design used by the compact toroid injection experiment.[10] The optical components are mounted on an aluminum structure with two extension arms which allow the system to straddle the vacuum chamber, as shown in Fig. 1. The laser beam is modulated using an acousto-optic modulator (AOM) (Intra-Action ATM-A1) operating at 110 MHz, which also serves as a beamsplitter. The undeflected beam is used as the scene beam, and the deflected beam (modulated at 110 MHz) is the reference beam. The scene beam makes a double pass through the plasma and also through a quarter wave plate, rotating the angle of polarization by $\pi/2$, so that on returning to the polarizing beamsplitter (1) it is deflected onto a second beamsplitter (2) where it is recombined with the reference beam. The combined beam is then passed through a polarizer which projects the polarization of the two beams onto a common axis intermediate between the polarization of the two component beams. Detection of the modulated interference signal is via a reverse biased *PIN* diode (Thorlabs DET10A).

The signal from the *PIN* diode is passed to a quadrature heterodyne detector where it is resolved into two components proportional to the sine and cosine of the phase difference between the scene and reference beams. These signals are digitized at 25 MHz with a total record length of 2500 points, giving a time window of 100 μs. Prior to analysis the raw data were filtered using a fast Fourier transform cutoff frequency of 1 MHz. All data presented here have a time resolution of 1 μs.

The accelerator is connected to a short bronze drift section containing feedthroughs for magnetic probes. The bronze drift section is in turn connected to an octagonal vacuum chamber as shown in Fig. 2, with large transparent top and bottom windows. The interferometer arms extend above and below this vacuum chamber such that the scene

 © 2010 American Institute of Physics

Author complimentary copy. Redistribution subject to AIP license or copyright, see http://php.aip.org/php/copyright.jsp

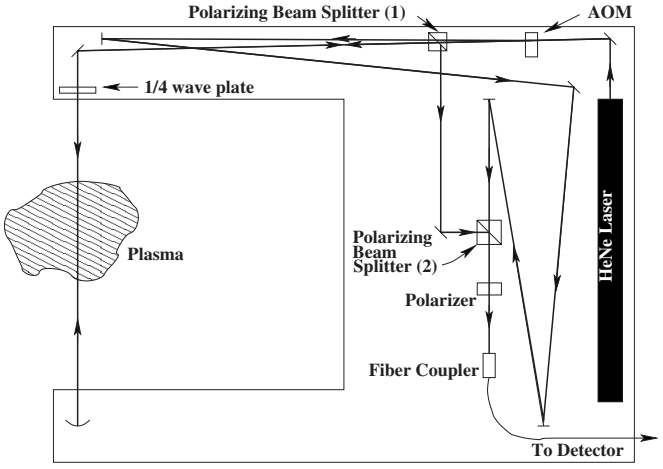

FIG. 1. Schematic of the interferometer layout. The beam from the HeNe laser is passed through the AOM which splits it into two beams, an unmodulated beam (the scene beam) and a reference beam modulated at 110 MHz. The scene beam makes two passes through the plasma and also through a quarter wave plate, which rotates the angle of polarization through $\pi/2$ so that it is reflected by polarizing beamsplitter 1 down onto the recombination beamsplitter 2, where it is recombined with the reference beam. The combined beam is passed to the photodiode via fiber, having passed through a polarizer which projects the scene beam and reference beam polarizations onto the same axis, intermediate between the two polarizations of the individual beams.

beam passes through the chamber at a point 15 cm from where the plasmoid enters, and centered on the plasmoid trajectory. Additional diagnostics include fast imaging using a PIMax framing camera from Princeton Instruments which is capable of shutter speeds down to 5 ns, a fast pressure probe for measurements of plasmoid stagnation pressure, and an 1 m Czerny–Turner spectrometer which is used for Doppler measurements of plasmoid velocity and Stark measurements of electron density.

The results presented here are from a single experimental run on November 1 and 5 of 2007, consisting of 19 shots taken at a base pressure of 2×10^{-5} Torr. The capillary injector bank consisted of eight 0.15 μF capacitors at 35 kV, the accelerator bank of nine 14 μF capacitors charged to 18 kV, yielding a peak accelerator current of 180 kA, with a pulse width of 22 μs. This accelerator was subsequently

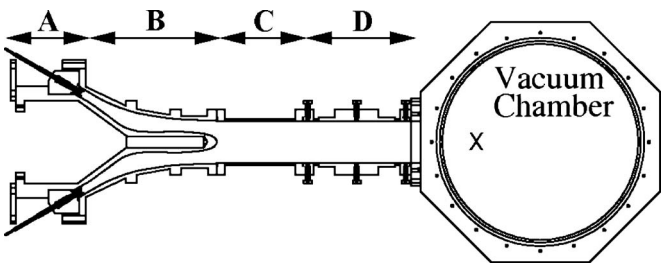

FIG. 2. Schematic of accelerator showing capillary injectors (a), coaxial section (b), pinch section (c), drift section (d), and vacuum chamber, viewed from above. The observation volume is shown by the *X*. For scale, the outside width of the octagonal vacuum chamber is 56 cm, the inner diameter is 45.7 cm.

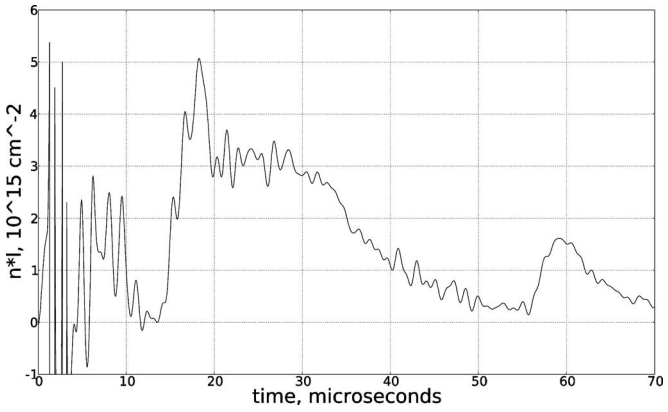

FIG. 3. A typical interferometer measurement of line integrated density. The signal prior to 12 μs is dominated by noise, with the plasma signal arriving at about 14 μs. The smaller peak near 60 μs is due to a second smaller plasmoid fed by residual plasma trickling out of the capillary injectors and ejected by ringing of the capacitor bank as seen in Fig. 4.

mounted on the Maryland centrifugal experiment[11] in a somewhat different configuration to test the possibility of driving plasma rotation.[9]

III. PHENOMENOLOGY

A typical measurement of line integrated density for this run is shown in Fig. 3, where the zero of the time axis is at the firing of the capillary plasma injectors. The majority of interferometer traces closely resemble this one, with a few showing significant variation as discussed below. The initial burst of activity right after firing the capillaries is due to noise, and is present even when the interferometer beam does not intersect the plasmoid path. Under these conditions the period after the initial burst of noise is quiescent, indicating that the signal after about 10 μs is relatively noise free. The sharp rise near 15 μs corresponds to the arrival of the plasma at the location of the interferometer observation volume, as verified by high speed photography and fast pressure probe measurements.[12] Following the sharp rise there is a period of slow variation, followed by a gentle fall back toward zero density. The feature appearing at approximately 55 μs is a second plasmoid ejected from the gun due to ringing of the capacitor bank, as shown in Fig. 4.

There is considerable variation in the gross features of the interferometer signal. Some traces show a single well defined sharp peak, some a very broad peak, and some a double peaked distribution. The four traces shown in Fig. 6 represent the full range of shapes seen in the data so far. Despite the considerable variation in gross shape of the traces, certain features are very consistent throughout the data, such as the arrival time of the plasmoid at the observation volume and the gentle fall of the density after passage of the main plasmoid mass. Further experimentation is needed to understand the source of this variation, though one possibility is that a large fraction of the plasmoid mass is contained in a toroid which is tilt unstable.

Figure 5 shows the results of a simulation of gun internal dynamics using the MACH2 2 1/2 d mhd code.[13] The density contours clearly show a concentration of mass at finite ra-

Author complimentary copy. Redistribution subject to AIP license or copyright, see http://php.aip.org/php/copyright.jsp

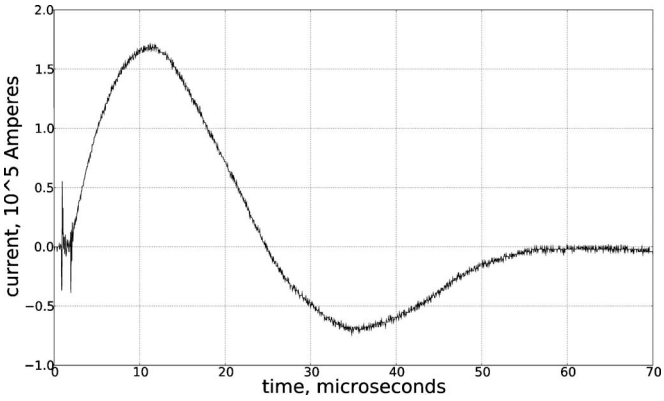

FIG. 4. A typical current trace. This trace is the main accelerator current for the shot shown in Fig. 3. The ringing of the bank ejects a second, smaller plasmoid late in time.

dius, showing that there is a toroidal structure in the mass distribution of the plasmoid in the late stages of the acceleration process. It is reasonable to suppose that this toroidal concentration of mass remains after the plasmoid has been ejected from the gun, at least for times which are short relative to the appropriate diffusive timescale. While magnetic field measurements indicate that the plasmoid contains some trapped flux, approximately 200 G, the plasma is highly collisional, with a Spitzer resistive decay time of approximately 2 μs (Ref. 9) inferred from B-dot probes in the drift section. These measurements show that the field is very turbulent, so we cannot characterize it further without additional experiments. Therefore we use a diffusion time scale due to thermal effects to estimate the persistence of structure in the plasmoid. Taking the temperature as 5 eV (from spectroscopy), mean ion mass as 4.7 amu [ablated polyethylene, $(CH_2)_n$], and transverse length scale as 10 cm, we obtain 10 μs for the thermal diffusion time scale. As this is longer than the transit time from the gun to the observation volume ($\sim$3 μs), structures present in the plasma as it exits the gun will not yet have diffused away.

In the case where the toroid does not tilt on exiting the gun, so that it passes through the observation volume with the laser beam parallel to the toroidal plane (i.e., parallel to the major radius of the toroid), the line integrated density would resemble the signal seen in Fig. 6(c). If the toroid tilts through $\pi/2$ prior to reaching the observation volume the line integrated density would resemble Fig. 6(d), with the traces of (a) and (b) representing intermediate cases.

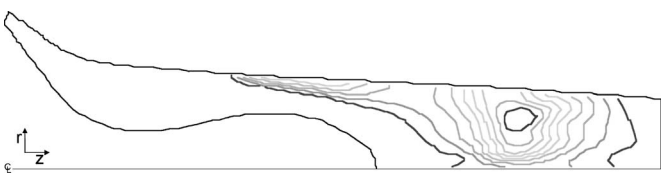

FIG. 5. MACH2 simulations show a toroidal mass concentration in the late stages of the acceleration process. This image shows only regions B and C of Fig. 2

IV. ANALYSIS

The arrival of the plasmoid at the observation location was identified with the beginning of the sharp rise after the initial burst of noise, and the end of the plasmoid was identified with the return of the signal to the baseline level. Identification of the end of the plasmoid is clearly subject to much wider uncertainty due to the gentle slope of the signal decay, but this turns out to have little effect on the analysis. The parameters of greatest interest are the total plasmoid mass, the rise time, and the peak density.

In order to obtain total particle number we have to integrate the plasma density over the plasmoid volume. The quantity measured by the interferometer is the line integrated density

$$n_l = 2\int_0^{R_0} n(r)dr,$$

where the factor of two is due to the fact that the laser beam traverses the entire plasmoid, not just the region from the axis to R_0, the effective outer edge of the plasmoid. To obtain the total plasmoid mass we want

$$M_{\text{tot}} = \bar{m}_i \int_0^{z_0}\int_0^{2\pi}\int_0^{R_0} n(r,\theta,z) r dr d\theta dz, \tag{1}$$

$$= \bar{m}_i \pi a \int_0^{z_0} n_l(z) dz, \tag{2}$$

where $\bar{m}_i$ is the mean ion mass, a is the transverse scale length of the plasma, and we have assumed azimuthal symmetry. Since the observation volume is fixed, we assume a constant velocity of the plasmoid, so that $dz \rightarrow v dt$. Measurements using spectroscopy and fast imaging indicate that the plasmoid velocity from this accelerator is typically about 90 km/s. However, this series of experiments was conducted with an additional instrumented drift section between the accelerator and the vacuum tank, which reduced the plasmoid velocities to about 70 km/s, so this value was used in all further analysis. Fast imaging indicates a plasmoid diameter of approximately 10 cm, which is consistent with the diameter of the accelerator bore at the exit plane, so this value was used for a.

The start of the plasmoid is identified by locating the point where the signal rises to 1/4 of the peak value, and then searching backward in time to find the first minimum. The end of the plasmoid is identified with the point at which the relative contribution of the next data point to the total integrated signal falls below 0.0002, which results in the end point being shortly before the arrival of the second plasmoid. The signal has not returned to zero by this point, but the second plasmoid always arrives before the return of the signal to zero, so there will inevitably be some underestimate of the plasmoid mass if the second plasmoid is excluded. The arbitrary ratio of 0.0002 was chosen because it reliably excludes the second plasmoid while at the same time including nearly all of the first plasmoid.

The main quantity of interest is the total plasmoid mass, which is obtained by assuming that the ionic composition is

Author complimentary copy. Redistribution subject to AIP license or copyright, see http://php.aip.org/php/copyright.jsp

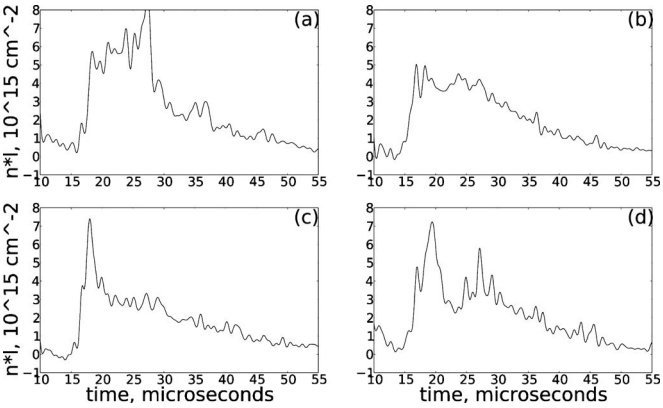

FIG. 6. Four traces showing the range of plasma signals seen in the data.

two protons for every carbon ion, corresponding to the molecular structure of the high density polyethylene used in the ablative capillaries. This assumption gives a value for $\bar{m}_i$ of 4.7 amu per ion. Additional quantities of interest are the full width at half maximum (FWHM), the total plasmoid length, the rise time, and the time at which half of the plasmoid mass has passed the observation volume, which along with total duration, gives a measure of the symmetry of the plasmoid shape. The rise time is here defined as the time taken to rise from 1/4 to 3/4 of the peak value. This is chosen over the more common 10–90% of peak value because the location of the peak moves around a lot, while the sharp rise associated with the plasmoid arrival is fairly consistent, as may be seen in Fig. 6.

Using the methods described above, the mean plasmoid mass is 58 ± 9 μg, with a FWHM of 13 ± 5.8 μs, total duration of 34 ± 2.4 μs, and a rise time of 2.3 ± 1.5 μs. The mean time taken for half the mass to arrive is 11.3 ± 1.2 μs. No detailed analysis was made of the second plasmoid, but rough analysis indicates a total mass of approximately 12 μg.

Recent results using an upgraded interferometer and a modified gun that uses spark gaps to inject the preionized plasma show peak densities above 1.5×10^{15} cm^{-3}. Additional experiments will be needed to verify that the plasmoid reproducibility is as good as the results presented above, but initial results are promising.

Measurements of total plasmoid momentum using a simple ballistic pendulum technique give total plasmoid momentum in this configuration of 10 g m s^{-1}, which corresponds to a total integrated mass for both plasmoids of 111 μg, using the nominal velocity of 70 km/s. This is higher than the mass derived from interferometry by 46%, most likely due to a "rocket effect" of ablated material from the pendulum itself.

V. DISCUSSION

The most striking feature of the results is the large spread in the FWHM values, which reflects the diversity of traces shown in Fig. 6. Despite this large spread in FWHM the arrival times for half the mass are quite tightly clustered, as are total duration and mean plasmoid mass. This suggests fairly good reproducibility of the plasmoid, with some variation in morphology. Using the velocity estimate of 70 km/s for the plasmoid, the time measurements can be converted into lengths, so we can infer that half the plasmoid mass is concentrated in the leading 75 cm of the plasmoid, with the total plasmoid length being just under 2.3 m, most of which is a long low density tail.

Further investigation will focus on resolving the source of the spread in the FWHM measurements as well as exploring the radial density profile of the plasmoid. Both of these aims will be facilitated by the addition of a second channel to the interferometer.

These early tests of the coax gun utilized relatively low current (180 kA). However, to achieve higher density and more compact jet lengths, these tests must be repeated with higher current, shorter pulse width, and with more mass injected via the capillaries. Since the set of measurements described in this paper were taken, the plasma guns have evolved considerably in performance, which will be the subject of future papers. The full-scale gun, for example, is designed to operate at close to 1 MA peak current, with pulse widths of only 8–10 μs and should thus provide densities above 10^{16} cm^{-3}.[3] Initial testing of this plasma gun has just begun.

VI. CONCLUSIONS

We have presented interferometric data and analysis of an early set of test runs at modest current and total plasma mass. The plasmoids in these tests consistently delivered a plasmoid in the range of 58 μg with good shot-to-shot repeatability. There is considerable variation in the gross structure of the plasmoid as seen by the interferometer, but the parameters of greatest importance for formation of a uniform plasma liner suitable for use in MIF experiments, namely total mass, rise time, and half-mass arrival time are well clustered. Future papers will examine profile characteristics of higher density, higher mass plasma jets achieved with higher current and injected mass.

ACKNOWLEDGMENTS

This research was supported by the DOE Office of Fusion Energy Science under Grant No. DE-FG02-05ER54810 and SBIR Grant Nos. DE-FG02-04ER83978 and DE-FG02-05ER84189.

[1] J. Marshall, Phys. Fluids **3**, 134 (1960).
[2] K. Thom, J. Norwood, and N. Jalufka, Phys. Fluids **7**, S67 (1964).
[3] F. D. Witherspoon, A. Case, S. J. Messer, R. Bomgardner III, M. W. Phillips, S. Brockington, and R. Elton, Rev. Sci. Instrum. **80**, 083506 (2009).
[4] J. T. Cassibry, Y. C. F. Thio, and S. T. Wu, Phys. Plasmas **13**, 053101 (2006).
[5] A. V. Voronin, V. K. Gusev, Yu. V. Petrov, N. V. Sakharov, K. B. Abramova, E. M. Sklyarova, and S. Yu. Tolstyakov, Nucl. Fusion **45**, 1039 (2005).
[6] T. E. Markusic, Y. C. F. Thio, and J. T. Cassibry, Proceedings of the 38th AIAA Joint Propulsion Conference AIAA-2002–4125, Indianapolis, IN, 2002.
[7] T. M. York, C. Zakrzwski, and G. Soulas, J. Propul. Power **9**, 553 (1993).
[8] C. J. Michels and T. M. York, AIAA J. **11**, 579 (1973).

Author complimentary copy. Redistribution subject to AIP license or copyright, see http://php.aip.org/php/copyright.jsp

[9]I. Uzun-Kaymak, S. Messer, R. Bomgardner, A. Case, R. Clary, R. Ellis, R. Elton, C. Teodorescu, F. D. Witherspoon, and W. Young, Plasma Phys. Controlled Fusion **51**, 095007 (2009).
[10]K. L. Baker, D. Q. Hwang, R. W. Evans, R. D. Horton, H. S. McLean, S. D. Terry, S. Howard, and C. J. DiCaprio, Nucl. Fusion **42**, 94 (2002).
[11]R. F. Ellis, A. Case, R. Elton, J. Ghosh, H. Griem, A. Hassam, R. Lunsford, S. Messer, and C. Teodorescu, Phys. Plasmas **12**, 055704 (2005).
[12]S. Messer, A. Case, R. Bomgardner, M. Phillips, and F. D. Witherspoon, Phys. Plasmas **16**, 064502 (2009).
[13]R. E. Peterkin, M. H. Frese, and C. R. Sovinc, J. Comput. Phys. **140**, 148 (1998).

Author complimentary copy. Redistribution subject to AIP license or copyright, see http://php.aip.org/php/copyright.jsp